Earth and Space Science

RESEARCH ARTICLE
10.1029/2021EA002193

The Relation of Environmental Conditions With Charge Structure in Central Argentina Thunderstorms

Bruno L. Medina[1,2], Lawrence D. Carey[1], Phillip M. Bitzer[1], Timothy J. Lang[3], and Wiebke Deierling[4]

[1]Department of Atmospheric and Earth Science, The University of Alabama in Huntsville, Huntsville, AL, USA, [2]Ann and H. J. Smead Department of Aerospace Engineering Sciences, University of Colorado Boulder, Boulder, CO, USA, [3]NASA Marshall Space Flight Center, Huntsville, AL, USA, [4]University of Colorado Boulder, Boulder, CO, USA

Abstract In this study we explored the environmental conditions hypothesized to induce a dominant charge structure in thunderstorms in the province of Cordoba, Argentina, during the RELAMPAGO-CACTI (Remote sensing of Electrification, Lightning, And Mesoscale/microscale Processes with Adaptive Ground Observations-Clouds, Aerosols, Complex Terrain Interactions) field campaigns. Hypothesized environmental conditions are thought to be related to small warm cloud residence time and warm rain growth suppression, which lead to high cloud liquid water contents in the mixed-phase zone, contributing to positive charging of graupel and anomalous charge structure storms. Data from radiosondes, a cloud condensation nuclei (CCN) ground-based instrument and reanalysis were used to characterize the proximity inflow air of storms with anomalous and normal charge structures. Consistent with the initial hypothesis, anomalous storms had small warm cloud depth caused by dry low-level humidity and low 0°C height. Anomalous storms were associated with lower CCN concentrations than normal storms, an opposite result to the initial expectation. High CAPE is not an important condition for the development of anomalous storms in Argentina, as no clear pattern could be found among the different parameters calculated for updraft proxy that would be consistent with the initial hypothesis.

Key Points:

- Dry low-level humidity and low freezing height led to small warm cloud depth and increased supercooled cloud water for anomalous storms
- Unlike other regions, high CAPE is not a necessary condition for the development of anomalous charge structure storms in Argentina
- Anomalous storms unexpectedly presented lower cloud condensation nuclei concentrations than normal storms

Supporting Information:

Supporting Information may be found in the online version of this article.

Correspondence to:

B. L. Medina,
bruno.medina@colorado.edu

Citation:

Medina, B. L., Carey, L. D., Bitzer, P. M., Lang, T. J., & Deierling, W. (2022). The Relation of environmental conditions with charge structure in central Argentina thunderstorms. *Earth and Space Science*, *9*, e2021EA002193. https://doi.org/10.1029/2021EA002193

Received 20 DEC 2021
Accepted 14 APR 2022

Author Contributions:

Conceptualization: Bruno L. Medina, Lawrence D. Carey
Data curation: Bruno L. Medina
Formal analysis: Bruno L. Medina, Lawrence D. Carey, Timothy J. Lang, Wiebke Deierling
Funding acquisition: Lawrence D. Carey, Phillip M. Bitzer, Timothy J. Lang, Wiebke Deierling
Investigation: Bruno L. Medina, Phillip M. Bitzer, Timothy J. Lang
Methodology: Bruno L. Medina, Lawrence D. Carey

1. Introduction

Environmental characteristics such as the temperature, humidity, CCN concentration, and wind field are fundamental in inducing cloud formation, microphysical processes, and kinematic motion within a cloud. These processes, in turn, affect hydrometeor charging polarity and, at a larger scale, the regions of charge that are developed inside thunderstorms (Carey & Buffalo, 2007; Eddy et al., 2021; Fuchs et al., 2015; Smith et al., 2000). Exploring charge structures is crucial as it relates to storm severity (Carey & Rutledge, 1998; Lang & Rutledge, 2011; MacGorman & Burgess, 1994), it impacts the production of nitrogen oxides (DeCaria et al., 2005; Price et al., 1997), affects the global electric circuit (Davydenko et al., 2004), lightning safety (Curran et al., 2000), etc.

From laboratory experiments, significant charge transfer at a particle level occurs during the rebounding collisions of a riming graupel particle with ice crystals in the presence of supercooled cloud liquid water (Saunders et al., 1991; Takahashi, 1978). The sign of charge transfer is dependent mainly on the temperature and the effective liquid water content, with graupel acquiring net positive charge for high temperatures and high liquid water contents because supercooled cloud water accretion heats the graupel particle, leading to sublimation of the surface and reduced diffusional growth (Berdeklis & List, 2001; Baker et al., 1987; Emersic & Saunders, 2010; Pereyra et al., 2000; Saunders et al., 1991, 2001; Saunders & Peck, 1998; Takahashi, 1978; Williams et al., 1991). Storm scale separation of hydrometeors is caused by terminal fall speed differences in the presence of a vertically varying updraft, which leads to a dominant charge region in the upper levels of a storm due to charged ice crystals and a charge region in the mixed-phase layer below due to charged graupel. Thunderstorms with dominant positive (negative) charge in the mixed-phase layer and upper level negative (positive) charge are referred to as anomalous (normal) charge structure storms (Bruning et al., 2014; Dye et al., 1986, 1988, 1989; Rust & MacGorman, 2002; Rust et al., 2005; Williams, 1985). Storms with enhanced low-level positive charge and negative charge at mid-levels are also often classified as anomalous (Bruning et al., 2014; Fuchs et al., 2015; Qie et al., 2005). The altitudes of charge layers are correlated with updraft speeds (Marshall et al., 1995; Stolzenburg, Rust, Smull, & Marshall, 1998), including for supercellular storms (Stolzenburg, Rust, & Marshall, 1998; Stolzenburg & Marshall, 2008), resulting in complex charge structures that vary relative to the updraft region

Project Administration: Lawrence D. Carey, Phillip M. Bitzer, Timothy J. Lang, Wiebke Deierling
Software: Bruno L. Medina
Supervision: Lawrence D. Carey, Wiebke Deierling
Validation: Bruno L. Medina
Visualization: Wiebke Deierling
Writing – original draft: Bruno L. Medina
Writing – review & editing: Lawrence D. Carey, Phillip M. Bitzer, Timothy J. Lang, Wiebke Deierling

(Bruning et al., 2010). Turbulent eddies in updraft regions are thought to produce small pockets of charge and small flash sizes (Bruning & MacGorman, 2013).

Because net positive charge on graupel in the mixed-phase layer is favored in an environment rich with supercooled cloud liquid water, we hypothesize the environmental conditions that are connected to the kinematic and microphysical processes, which lead to more cloud liquid water being transported from the warm region of a cloud to sub-freezing temperatures where charging occurs, are also related to the development of anomalous charge structures (Carey & Buffalo, 2007; Carey et al., 2003; Chmielewski et al., 2018; Fuchs et al., 2015; Williams et al., 2005).

It is intuitive to consider updraft strength as one of the physical processes that contribute to enhanced supercooled cloud liquid water contents in the mixed-phase layer. All else being equal, stronger updrafts would reduce cloud droplets residence time in the warm cloud depth, reducing time for growth by collision and coalescence, lifting droplets to sub-freezing temperatures, and contributing to the increase of the mixed-phase layer cloud liquid water content (Fuchs et al., 2015; Ziegler et al., 1991). Hence, a strong updraft is hypothesized to contribute to positive charging of graupel and the development of anomalously charged thunderstorms. High cloud base also contributes to stronger and wider updrafts, as the larger residence time of a parcel beneath the cloud base provides for more unstable air entrainment and a wider parcel (Mulholand et al., 2021). Also, large wind shear is thought to provide dynamical forcing for strong updrafts, contributing to the organization and longevity of storms, leading to anomalous charge structure storms (Carey & Buffalo, 2007). Low precipitable water integrated over the entire vertical depth would produce less rainwater loading of updrafts and thus stronger updrafts (Carey & Buffalo, 2007; Eddy et al., 2021; Emanuel, 1981; Knupp & Cotton, 1985), resulting in anomalous storms.

A shallow warm cloud depth (WCD) suppresses warm rain growth due to the low droplet residence time in this layer (Fuchs et al., 2015, 2018), resulting in droplets not developing sufficient differential fall speeds for growth by collision and coalescence. These conditions contribute to less precipitation fallout and a larger availability of small droplets in the WCD that can be lifted above the freezing level by an updraft, contributing to a larger cloud liquid water content in the mixed-phase layer (Carey & Buffalo, 2007; Fuchs et al., 2015, 2018; Williams et al., 2005). Dry air entrainment near the cloud base possibly acts to suppress droplet growth by collision and coalescence as well, contributing to more small droplets available in the WCD to be lifted to the mixed-phase layer (Chmielewski et al., 2018; Grant & van den Heever, 2015), contributing to positive charging of graupel and leading to anomalously charged storms.

An environmental condition that contributes to small WCD is low humidity at low levels, which results in the formation of a cloud base, or lifted condensation level (LCL), at a high altitude according to the parcel theory (Fuchs et al., 2018). Similarly, a low freezing level height could result in a small WCD. Then, because both dry low-level air and low altitude of the 0°C isotherm diminish WCD, these conditions are hypothesized to be associated with more small droplets in the WCD, more cloud liquid water transported to the mixed-phase layer, positive charging of graupel, and anomalous thunderstorms.

Lastly, a large CCN concentration is a condition hypothesized to contribute to more cloud droplets being nucleated and condensed in the warm cloud. More small droplets in the warm cloud leads to droplet growth suppression due to their similar fall speeds and increased competition for available water vapor. For a given updraft, these small droplets are more easily carried aloft, leading to a large cloud liquid water content in the mixed-phase layer, positive charging of graupel and anomalous storms (Albrecht et al., 2011; Fernandes et al., 2006; Lyons et al., 1998).

In southeast South America, a region that has some of the strongest thunderstorms with the largest flash rates in the world (Zipser et al., 2006), the RELAMPAGO-CACTI field campaigns were conducted with sounding, lightning, and multiple radar measurements in the Argentinian province of Cordoba during the 2018–2019 warm season (Nesbitt et al., 2021; Varble et al., 2021). These field projects provided a novel opportunity to study the meteorological environment and electrification of thunderstorms in this region. A characterization of Cordoba thunderstorms charge structure using five months of Lightning Mapping Array (LMA) data was provided in Medina et al. (2021), in which 13% of thunderstorms presented a predominant anomalous charge structure, with its main dipole consisting of the negative charge region located above the dominant positive charge region. Some of these anomalous storms had their main dipole located at low altitudes, with positive charge located in a temperature region warmer than −10°C and the absence of an upper-level positive charge. As shown in Medina

et al. (2021), these charge structure features were not observed in other regions such as in Colorado, where most anomalous thunderstorms were found to have their main positive and negative charge regions located in the mixed-phase layer and above, respectively. Hence, there is a vital importance in better characterizing the environment conducive to Cordoba anomalous charge structure thunderstorms and compare those to a control set of normal charge structure thunderstorms. As these thunderstorms have differing charge structure characteristics, which possibly combines a varying and different set of environmental ingredients, we study these thunderstorms and their environment in order to expand our understanding of the conceptual model for thunderstorm charging.

We conducted a study of the Cordoba (Argentina) environmental conditions that contribute to different thunderstorm charge structure archetypes. Data from radiosondes that were launched during RELAMPAGO-CACTI (Nesbitt et al., 2021; Schumacher et al., 2021; Varble et al., 2021) were associated temporally and spatially to thunderstorms to determine if they were representative of the inflow air to the updraft of a normal or anomalous charge structure storm. From these inflow proximity soundings, various environmental parameters were calculated, which are hypothesized to be related to certain charging regimes in the mixed-phase region of a storm as discussed earlier. CCN concentrations from a ground-based instrument for detection of CCN were also associated to storms when found to be representative of the storm environments. We also characterized the environments of thunderstorm charge structures observed during RELAMPAGO-CACTI using reanalysis data in order to facilitate the analysis of a larger set of events and thereby confirm the outcomes of the sounding analysis.

2. Data and Methodology

Datasets from the RELAMPAGO-CACTI Extensive Operational Period (EOP) from November 2018 to April 2019 (Nesbitt et al., 2021; Varble et al., 2021) were used in this study. Output from an automated method presented in Medina et al. (2021) to predict regions of charge from LMA flashes (hereafter referred to as Chargepol) was used to determine the predominant charge structure (i.e., normal or anomalous) in thunderstorms. Chargepol estimates altitude and vertical depth of positive and negative charge layers from a lightning flash, and when applied to many flashes over extended periods of time, can infer the structure (including main dipoles and tripoles) and evolution of charge within a thunderstorm (Medina et al., 2021). Hence, for a given storm, the altitude modes for positive and negative charge for the entire storm life cycle were obtained. If the positive mode altitude was higher (lower) than the negative mode altitude, the event was characterized as a normal (anomalous) charge structure, highlighting the predominance of positive (negative) charge detected above negative (positive) charge, in a similar approach to the Medina et al. (2021) study. Figures 1a, 1c, and 1e show examples of Chargepol output from lightning flashes for a normal, an anomalous, and an anomalous storm with enhanced low-level positive charge with no upper positive charge layer (hereafter low-level anomalous storm). Figures 1b, 1d, and 1f show histograms with the probability density of layers from lightning flashes in relation to altitude, that is, the fraction of a polarity charge layer that propagated through each altitude bin. The positive and the negative altitude modes can be seen in these histograms as the positive and negative peaks, which are used to define the main charge structure of an event, as described above. This approach ensures the anomalous category encompasses storms with dominant positive charge layer located in the mixed-phase layer rather than in the high levels near the cloud top, which by itself characterizes charge structure as being not normal even when analyzed by other methods such as VHF altitude distribution. The majority of cases being considered are isolated or multicellular storms.

As storms with a predominant anomalous or normal charge structure were determined, a search on a data set of 2712 quality-controlled radiosondes launched during RELAMPAGO-CACTI EOP (Nesbitt et al., 2021; Schumacher et al., 2021; UCAR/NCAR–Earth Observing Laboratory, 2020; Varble et al., 2021) was performed to characterize the environment that would represent the proximity inflow air ingested to convective events. Soundings farther than 100 km from the storm initiation, soundings released with more than 6 hr prior to the event, and profiles contaminated by nearby cloud and precipitation, storm's outflow or other mesoscale boundary were discarded. Twenty-three soundings were found, 10 representing storms with predominant anomalous charge structure and 13 representing normal storm environments (Table 1). Out of the 10 anomalous events, 3 had the center of the positive charge altitude mode at a temperature warmer than −10°C, defining the low-level anomalous storms (LLA in Table 1) but still considered in the anomalous data set for statistical purposes in this study. Figure 2 show the chosen sounding profiles associated with the three storm examples shown in Figure 1. Only two soundings were launched 3–4 hr before the first lightning flash of an event, and all others were within

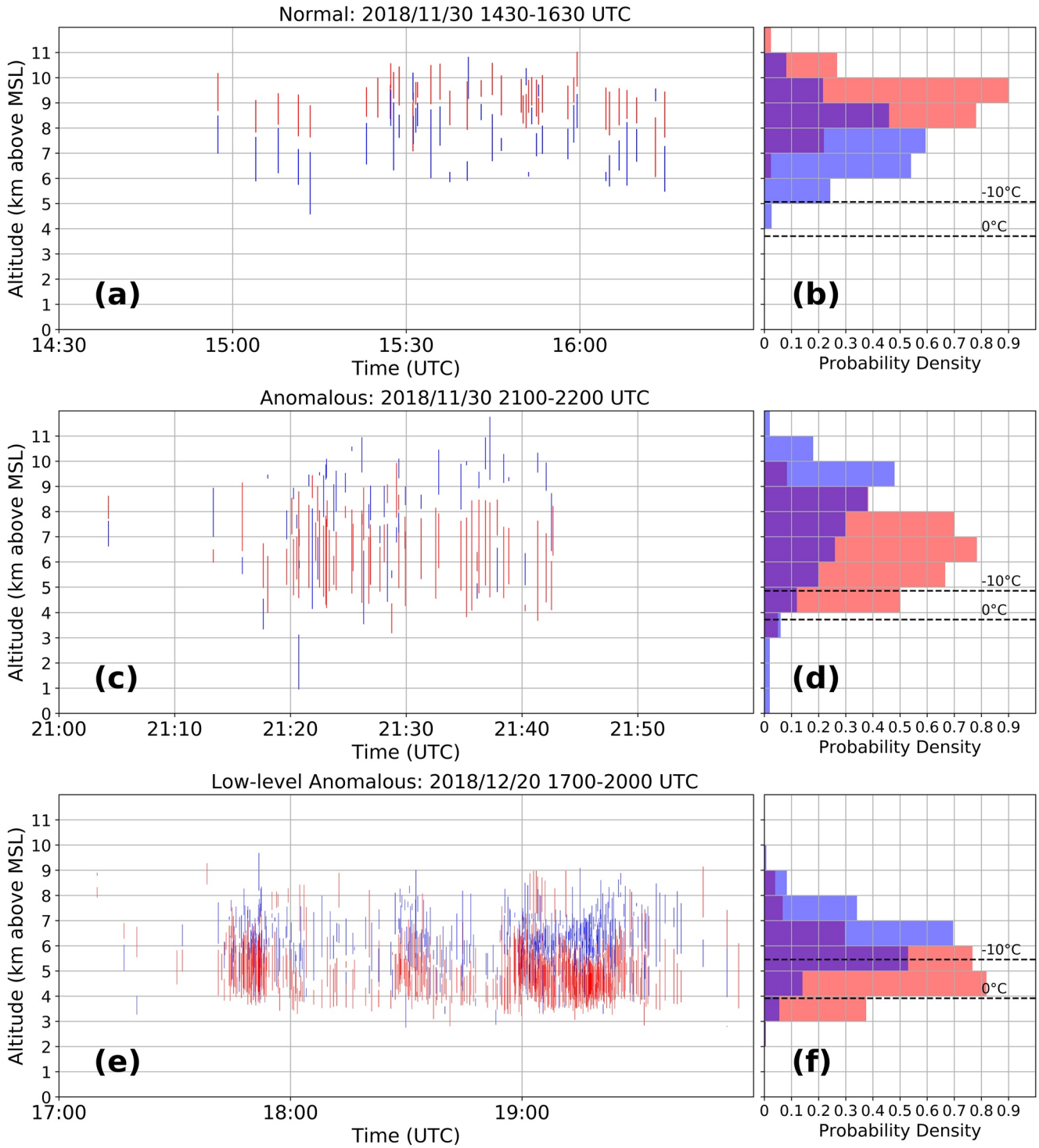

Figure 1. Charge layers estimated from flashes using the Chargepol automated method for: (a) a normal storm on 30 November 2018 from 1400 UTC to 1700 UTC, (c) an anomalous storm on 30 November 2018 from 2100 UTC to 2200 UTC, (e) and a low-level anomalous storm on 20 December 2018 from 1700 UTC to 2000 UTC. Each red (blue) vertical line represents a positive (negative) charge layer estimated from a flash. (b), (d), (f) Histograms of probability density for charge layers detected from flashes for each storm, from which altitude modes are obtained to define the storm's charge structure. The 0°C and the −10°C isotherm heights are displayed in the histogram plots.

Table 1
The 13 Normal and 10 Anomalous Charge Structure Events, the Event's Dominant Charge Structure (A = Anomalous, LLA = Low-Level Anomalous and N = Normal), the Radiosonde Chosen to Represent the Storm's Environment, the Approximate Time and Distance of Each Sounding to the Storm's First Flash and Whether the CCN Ground Observation was Associated to the Event

Date	Dominant charge structure	Sounding name and time	Approximate time and distance from storm's first flash	CCN event?
11/29	A	UIUC1, 1603 UTC	−1h10 min, 29 km	Yes
11/30	LLA	Cordoba airport, 2327 UTC (11/29)	−3h45 min, 10 km	No
11/30	N	Cordoba airport, 1428 UTC	−30 min, 46 km	No
11/30	A	UIUC1, 2104 UTC	−10 min, 25 km	Yes
12/01	LLA	Cordoba airport, 2330 UTC (11/30)	−4h, 36 km	No
12/04	N	CSU, 1600 UTC	−1h, 16 km	Yes
12/05	A	SCOUT2, 1503 UTC	−2h, 10 km	Yes
12/11	N	Cordoba airport, 1603 UTC	−45 min, 75 km	No
12/11	N	Cordoba airport, 2200 UTC	−55 min, 40 km	Yes
12/13	A	SCOUT3, 2255 UTC	−10 min, 35 km	No
12/14	N	CSU, 0100 UTC	−38 min, 35 km	No
12/20	LLA	ARM M1, 1600 UTC	−1h30 min, 39 km	Yes
12/26	N	ARM M1, 1600 UTC	0min, 15 km	Yes
12/30	N	Cordoba airport, 0530 UTC	−1h, 0 km	Yes
01/02	N	ARM M1, 1500 UTC	−2h10 min, 15 km	Yes
01/08	A	ARM M1, 2000 UTC	0min, 50 km	Yes
01/23	N	ARM M1, 1500 UTC	−1h, 5 km	Yes
01/25	N	ARM M1, 1500 UTC	−2h10 min, 0 km	Yes
01/29	N	ARM M1, 1500 UTC	−2h10 min, 10 km	Yes
02/08	N	ARM M1, 1800 UTC	−2h, 10 km	Yes
02/22	N	ARM M1, 1800 UTC	+10 min, 36 km	Yes
03/07	A	ARM M1, 1800 UTC	−1h, 64 km	Yes
03/14	A	ARM M1, 1500 UTC	−3h, 25 km	Yes

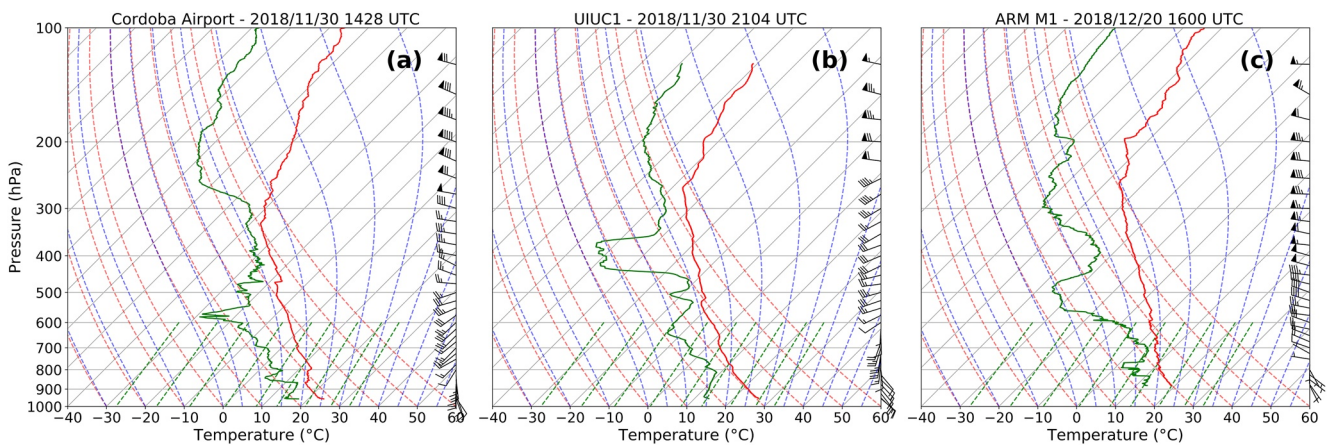

Figure 2. Soundings associated to each event shown in Figure 1: (a) Cordoba airport sounding on 30 November 2018 at 1428 UTC, (b) UIUC1 sounding on 30 November 2018 at 2104 UTC, and (c) ARM M1 sounding on 20 December 2018 at 1600 UTC.

Table 2
The 27 Normal and Seven Anomalous Charge Structure Events Used in the GEOS-5 FP Reanalysis Study, the Time and Location Used to Retrieve the Environmental Profile From Reanalysis and the Dominant Charge Structure (A = Anomalous, LLA = Low-Level Anomalous and N = Normal)

Reanalysis date and time	Grid point center latitude and longitude	Dominant charge structure
11/22, 0900 UTC	−31.25, −63.748	N
11/26, 0000 UTC	−32.5, −64.372	N
11/29, 1500 UTC	−32, −64.684	A
11/30, 1200 UTC	−31, −64.372	N
11/30, 2100 UTC	−31.75, −64.684	A
12/01, 0000 UTC	−31.75, −64.06	LLA
12/04, 1500 UTC	−31.25, −64.684	N
12/11, 2100 UTC	−31.25, −65	N
12/17, 1500 UTC	−31.25, −64.684	N
12/19, 1500 UTC	−32, −64.684	N
12/26, 1500 UTC	−32, −64.684	N
12/27, 0600 UTC	−32.5, −64.06	N
12/28, 0300 UTC	−31.75, −65	N
12/28, 1500 UTC	−31.75, −64.684	N
12/30, 0300 UTC	−32.25, −64.06	N
01/08, 1500 UTC	−31, −64.06	A
01/09, 1200 UTC	−31.75, −63.748	N
01/17, 0300 UTC	−31, −64.06	N
01/23, 0000 UTC	−32, −64.372	N
01/23, 1500 UTC	−32, −64.684	N
01/29, 2100 UTC	−32.5, −64.06	N
01/31, 1500 UTC	−31.5, −65	N
02/11, 0000 UTC	−32.25, −64.372	N
02/22, 1500 UTC	−32, −64.684	N
02/27, 1800 UTC	−32.5, −64.684	A
03/03, 1800 UTC	−32, −64.684	N
03/04, 0300 UTC	−32.5, −63.748	N
03/05, 1200 UTC	−31.5, −63.124	N
03/07, 1800 UTC	−31.75, −64.06	A
03/14, 1500 UTC	−31.75, −64.372	A
03/15, 0000 UTC	−32, −64.684	N
03/15, 1200 UTC	−31.75, −64.684	N
03/16, 0300 UTC	−31, −64.684	N
04/15, 0600 UTC	−31.75, −63.748	N

Note. Events in bold are events also included in the sounding data set.

3 hours. Similarly, three soundings occurred from 50 to 75 km from the storm's first lightning flash, while all others occurred within 50 km distance from the storm's first lightning flash.

Environmental parameters were calculated from the chosen soundings using the MetPy Python package (May et al., 2020). Calculated parameters included: surface equivalent potential temperature, average specific (and relative) humidity for the layer between the surface and the LCL to assess low-level humidity that would affect LCL and WCD, LCL altitude, height of the 0°C isotherm, WCD, average specific (and relative) humidity for the WCD to assess the possible role of low-level dry entrainment near cloud base, precipitable water, surface-based (and most-unstable parcel) convective available potential energy (CAPE) for a proxy of updraft intensity, and 0–3 km (and 0–6 km) wind shear (Carey & Buffalo, 2007). Among the 23 chosen soundings, only one was truncated at a lower altitude than the equilibrium level, hence underestimating its surface-based and most-unstable CAPE values to 3,318 and 3527 J kg^{-1}, respectively. Another full sounding launched nearby at the same time had both CAPE values of 3645 J kg^{-1}, resulting in a likely underestimation of a few hundreds of J kg^{-1} for the utilized sounding.

Reanalysis data from NASA Goddard Earth Observing System Version 5 Forward Processing (GEOS-5 FP, Lucchesi, 2018) with 3-hr time resolution and 0.25° × 0.3125° grid spacing was obtained in order to calculate the same environmental parameters as in the sounding analysis. This analysis was performed in an attempt to increase the sample size of events in the data set and to thereby assess the representativeness of the sounding results. For a given thunderstorm, a profile was retrieved from the location where the event was initiated and at the closest reanalysis time step that occurred prior to the event initiation time. In cases the profile was clearly contaminated by clouds and precipitation, the previous time step was used (if not contaminated). For this reason, many potential events had to be discarded, leading to a smaller number of anomalous events in the reanalysis data set than in the sounding analysis. Seven anomalous events and 27 normal events were found and are shown in Table 2. It is important to note that most of these reanalysis events (21) in Table 2 are different from the sounding events in Table 1. Hence this reanalysis work is a nearly independent verification of the sounding analysis results.

In order to associate the concentration of CCN to storms with different charge structures, the Dual Column CCN Counter instrument located at the DOE ARM mobile facility site in Villa Yacanto (Uin et al., 2018; Varble et al., 2021) was used. The ramping mode averaged data is used in this study, which averages aerosol and CCN concentration at six different supersaturation values ranging from about 0.05% to about 0.95%. Then, for each day, this data set provides 96 observations (taken in a few hours) of average aerosol and CCN. Since the instrument accuracy decreases for supersaturation smaller than 0.1% and close to 100% of particles get activated at 1% supersaturation (Uin et al., 2018), we then use 0.55% in this study as it is representative of in-cloud supersaturation. CCN concentration measurement at a constant supersaturation of 0.55% prior to the storm initiation and not lowered by rainfall due to wet deposition of CCN was used. As this instrument provides a measurement at a fixed ground site during a limited period, fewer events were found to be characterized by this data set (7 anomalous and 10 normal events, Table 1).

Aerosol concentration estimated from Modern-Era Retrospective Analysis for Research and Applications, version 2 (MERRA-2, Gelaro et al., 2017) reanalysis is used to provide a larger data set and an independent verification of the Dual Column CCN Counter results. Events from this analysis are the same 34 events as in the GEOS-5

FP reanalysis. Following Stough et al. (2021), aerosol mixing ratio data from dust (0.1–1.8 μm), hydrophilic organic carbon with size of 0.35 μm, hydrophilic black carbon with 0.35 μm size, sea salt (0.1–1.5 μm), and sulfate with 0.35 μm size was converted to mass concentration at various pressure levels. It is important to note that this approach only provides a rough estimate of CCN, as no reliable methods for the retrieval of CCN are known from this type of aerosol data. Satellite-based aerosol reanalysis data is widely used as the only aerosol estimator available in various thunderstorm studies (e.g., Stough et al., 2021). Hence, it is important to compare the environmental outcomes associated with specific thunderstorm charge structure archetypes obtained using this aerosol estimate to those obtained using a ground-based measurement of CCN.

A comparison of anomalous and normal datasets for each environmental parameter calculated is performed by obtaining the Mann-Whitney U-statistic, a nonparametric test that does not need an assumption of the parent distribution of the data (Wilks, 2011). It is important to mention that we have also performed the two sample Student's *t*-test (Wilks, 2011) for parameters in which a normal distribution for both datasets was not rejected at a 5% confidence level using the Anderson-Darling test (Stephens, 1974). However, because not all datasets had a normal distribution, and for those that had normal distribution its Student's *t*-test *p* value was highly correlated with the Mann-Whitney U-statistic *p* value, we chose to show the nonparametric test *p* value only in this study for simplicity. The *p* value obtained from the Mann-Whitney U-statistic can be interpreted as the likelihood that the null hypothesis that the samples are drawn from the same distribution is rejected, hence we expect *p* values lower than 0.05 to characterize datasets that are statistically distinct from each other.

3. Environmental Parameters From Radiosondes

The parameters calculated from soundings representing anomalous and normal storm environments are shown in Figure 3, and the mean, median, and the Mann-Whitney U-statistic *p* values are shown in Table 3. The three low-level anomalous storms (with positive altitude mode at a temperature warmer than −10°C) are highlighted in Figure 3 in order to differentiate them from anomalous storms that present positive altitude mode at a temperature colder than −10°C. Nonetheless, all types of anomalous storms are considered in the same category for statistical analysis because of the small sample size.

In general, parameters associated with low-level humidity seem to explain the thunderstorms that assume an anomalous charge structure because its range of parameter values are consistent with hypothesized values when compared to normal storms. For example, the mean of surface equivalent potential temperature for anomalous events (338 K) is lower than the mean for normal events (359 K), with a Mann-Whitney U-statistic *p* value lower than 0.01 (Table 3). Another calculated parameter consistent with the hypothesized condition for anomalous storms was the average specific humidity for the layer between the surface and the LCL height, which showed a lower mean for anomalous events (10.1 g kg^{-1}) than for normal storms (14.8 g kg^{-1}) with *p* value lower than 0.01 as well. For the average of the relative humidity throughout the same layer, the mean was lower for anomalous (65%) than for normal (72%) storms, but the inter-quartile ranges presented a large overlap (Figure 3c).

As expected from the low-level humidity behavior, the LCL height mean was higher for anomalous (2,059 m) than for normal (1,834 m) storms. However, its *p* value was not lower than 0.05 as desirable (Table 3). Anomalous and normal samples are distinct for both WCD and height of 0°C parameters, with anomalous storms having lower values for both parameters (Figures 3e-3f). Higher LCLs combined with shallow WCD leads to a greater abundance of cloud droplets in sub-freezing temperature ranges, which results in more positively charged graupel and thus anomalous charge structures, per previous laboratory results.

Average specific humidity in the WCD was lower for anomalous storms (5.4 g kg^{-1}) than for normal storms (7.4 g kg^{-1}), with its *p* value lower than 0.01, suggesting dry air entrainment could have influenced microphysical conditions within anomalous storms more than normal storms in this layer. P value of 0.598 for average relative humidity in the WCD indicate that anomalous and normal samples were similar, as visible from the overlap of the inter-quartile range (Figure 3h). Since the low-to-mid levels of the troposphere presented low humidity for anomalous storms, the precipitable water, which consists of the vertical integration of water vapor mixing ratio, reflects this behavior. Hence, anomalous events presented lower mean precipitable water (25 vs. 35 mm for normal events) and the *p* value was lower than 0.01, consistent with the initial hypothesis where lower precipitation loading would favor stronger updrafts for anomalous events. However, both CAPE parameters showed lower means for anomalous storms with low *p* values (Table 3), contrary to the hypothesis that states that stronger

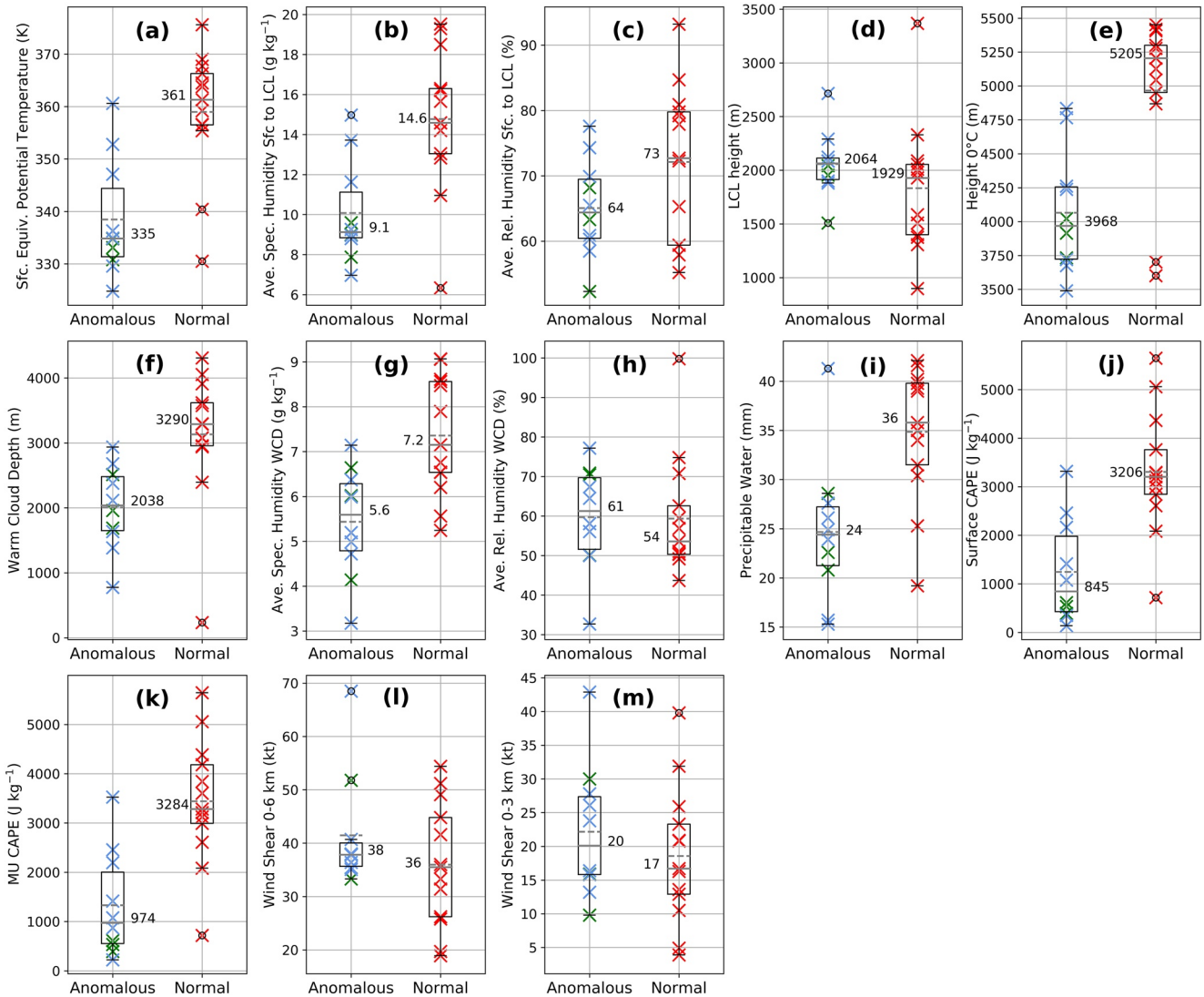

Figure 3. Box plots and values of environmental parameters (X's) calculated from soundings associated with normal (red), anomalous (blue), and low-level anomalous (green) storms for: (a) Surface equivalent potential temperature, (b) average specific humidity from the surface to LCL, (c) average relative humidity from the surface to LCL, (d) LCL height, (e) height of 0°C isotherm, (f) WCD, (g) average specific humidity for the WCD, (h) average relative humidity for the WCD, (i) precipitable water, (j) surface CAPE, (k) most-unstable CAPE, (l) wind shear from 0 to 6 km, and (m) wind shear from 0 to 3 km. Mean values are shown as gray dashed lines, and median values as horizontal gray lines along with its numerical value.

updrafts would be observed for anomalous storms. As initially hypothesized, wind shear parameters presented larger mean for anomalous than for normal storms (Table 3), but with high p values and substantial inter-quartile overlap (Figures 3l–3m).

4. Environmental Parameters From GEOS-5 FP Reanalysis

Figure 4 shows environmental parameters found to represent a set of seven anomalous and 27 normal events using the GEOS-5 FP reanalysis. Table 4 shows the mean and median for all parameters and the statistical test p values.

All low-level humidity parameters (surface equivalent potential temperature, average specific humidity and relative humidity from the surface to the LCL) showed lower mean for anomalous storms than for normal storms, consistent with results from soundings, but with p values greater than 0.05 (Table 4). Similar to the sounding analysis, the height of 0°C presented a larger distinction between anomalous and normal samples when compared to the LCL height parameter, both contributing to the WCD. No significant difference was observed between

Table 3
Environmental Parameters Mean and Median Calculated From Soundings Associated With Anomalous and Normal Storms, Rounded to the Nearest Integer (Except for Specific Humidity Parameters)

Environmental parameters	Anomalous mean (median)	Normal mean (median)	Mann-whitney U-statistic *p* values
Surface Equiv. Pot. Temp.	338 (335) K	359 (361) K	**0.0021**
Ave. Spec. Hum. Sfc-LCL	10.1 (9.1) g/kg	14.8 (14.6) g/kg	**0.0057**
Ave. Rel. Hum. Sfc-LCL	65 (64) %	72 (73) %	0.1823
LCL height	2059 (2,064) m	1,834 (1,929) m	0.1824
Height 0°C	4065 (3,968) m	4966 (5,205) m	**0.0032**
Warm Cloud Depth	2007 (2,038) m	3,133 (3,290) m	**0.0014**
Ave. Spec. Hum. WCD	5.4 (5.6) g/kg	7.4 (7.2) g/kg	**0.0039**
Ave. Rel. Hum. WCD	60 (61) %	59 (54) %	0.5980
Precipitable Water	25 (24) mm	35 (36) mm	**0.0069**
Surface CAPE	1247 (845) J/kg	3,307 (3,206) J/kg	**0.0021**
Most-unstable CAPE	1331 (974) J/kg	3,442 (3,284)	**0.0017**
Wind Shear 0–6 km	41 (38) kt	36 (36) kt	0.2916
Wind Shear 0–3 km	22 (20) kt	19 (17) kt	0.4382

Note. Mann-Whitney U-statistic *p* values are shown for all parameters. P values lower than 0.05 are bolded.

anomalous and normal storms for the LCL (Table 4), while *p* values for both 0°C height and WCD parameters were lower than 0.01. Consistent with the initial hypothesis and with sounding analysis results, both specific and relative humidity in the WCD parameters showed lower values for anomalous events, but only the average specific humidity parameter presented a *p* value lower than 0.05. Among all updraft proxy parameters (Figures 4i–4m), only precipitable water presented a low *p* value, indicating their anomalous and normal samples are distinct. Samples of the CAPE and wind shear parameters were not significantly different (Table 4).

Even though the results from the GEOS-5 FP reanalysis presented larger statistical test *p* values than the results from the soundings, these results are found to be qualitatively consistent with the results from the sounding analysis shown in the previous section. It is important to emphasize that few of these parameters presented a high confidence level that samples are distinct. Even so, an analysis of the general patterns in these results is provided below.

Anomalous storms presented lower values for the low-level humidity parameters, higher LCL height, lower 0°C height, and smaller WCD, which is consistent with the hypothesis that these conditions lead to lower droplet residence times in the WCD, less differential fall speeds between particles, more cloud liquid water content available in the mixed-phase layer, contributing to positive charging of graupel and anomalous storms. Anomalous storms with lower humidity in the WCD is also consistent with possible dry entrainment effects in this layer contributing to droplet growth suppression, more small droplets available that can be lifted to the mixed-phase layer, leading to anomalously charged storms. Lower values for precipitable water for anomalous storms is associated with stronger updrafts, just as initially hypothesized. However, all other parameters that infer kinematic motion (surface-based CAPE, most-unstable CAPE, 0–6 km wind shear, and 0–3 km wind shear) presented no clear distinction between anomalous and normal storms.

5. Analysis of CCN Concentration

CCN measurements at 0.55% supersaturation from the Dual Column CCN Counter instrument were found that represent seven anomalous and 10 normal events. Anomalous mean CCN concentration (1,134 cm^{-3}) was lower than for normal events (1,535 cm^{-3}) although with Mann-Whitney U statistic *p* value of 0.13. The anomalous inter-quartile range was also lower than for the normal events (Figure 5a). MERRA-2 estimates of aerosol concentration, more widely used for climatological purposes, is used here for a loose inference of CCN concentration using the methodology described in Section 2. Estimates for all 34 reanalysis events are shown in Figure 5b at different pressure levels, along with the average and standard deviation for the set of normal and anomalous

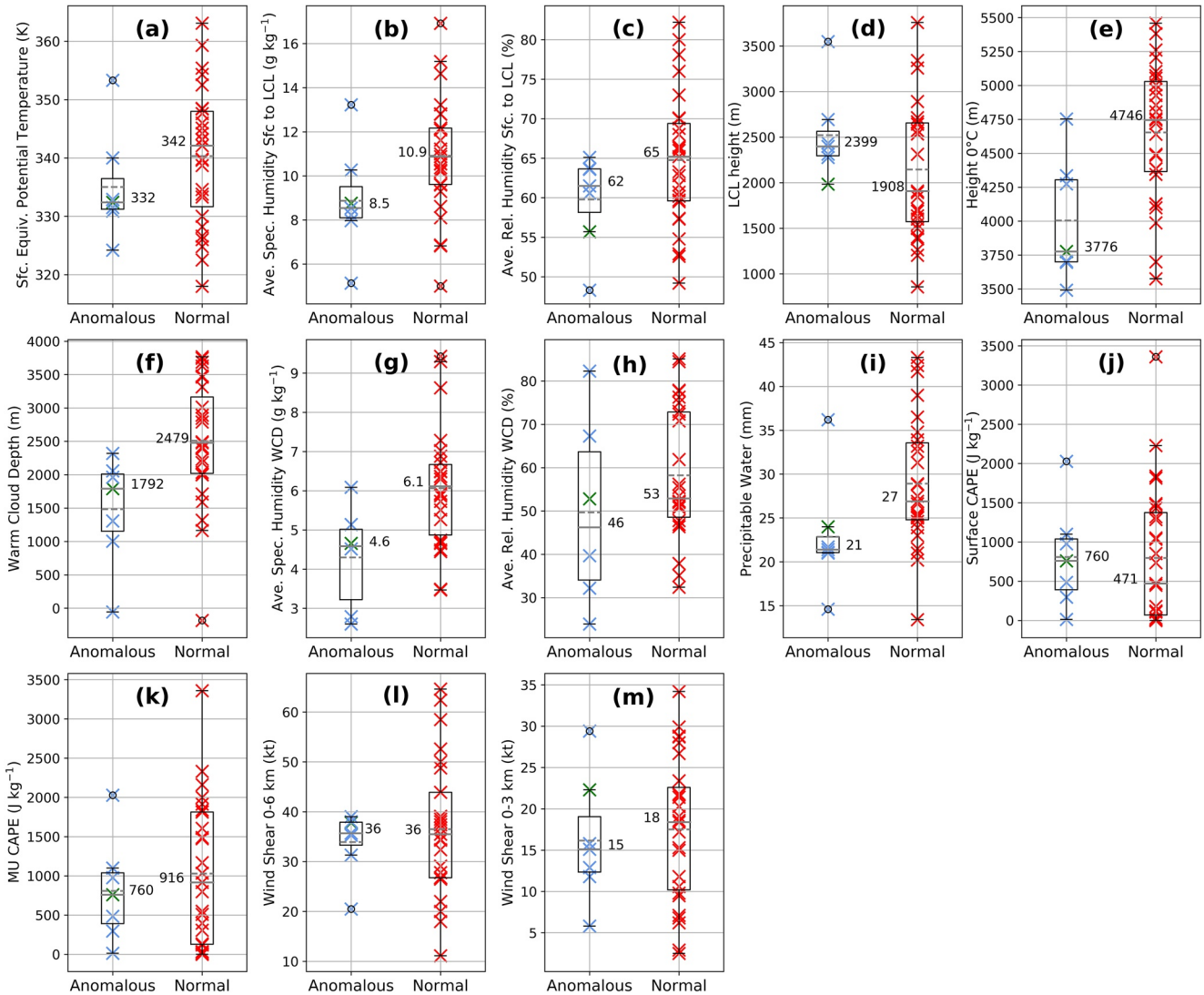

Figure 4. Same as in Figure 3 but for parameters estimated from GEOS-5 FP reanalysis.

storms. The average aerosol concentration for anomalous storms was also found to be lower than for normal storms in the low-level troposphere. The aerosol concentration from the MERRA-2 lowest level is shown in Figure 5c in order to provide a rough comparison of relative trends with the ground-based Dual Column CCN Counter observations, although the measurements being compared are completely different. Anomalous storm aerosol concentrations were also lower, with means equal to 6.2 μg m^{-3} and 10.7 μg m^{-3} for anomalous and normal storms, respectively. The Mann-Whitney U statistic *p* value calculated for this parameter was 0.115, larger than the threshold of 0.05. Although the findings from these two sets of aerosol data did not provide statistically significant differences between anomalous and normal datasets, the lower mean for anomalous storms is opposite to the initially expected result, where larger CCN concentration was expected for anomalous storms as it would induce more small droplets to be activated and larger cloud liquid water content to be ingested into the mixed-phase layer.

6. Summary and Discussion

This study presented the environmental conditions that indirectly influenced charge structure in Argentinian thunderstorms during the RELAMPAGO-CACTI field programs. Analysis of soundings launched nearby storms found to represent storm inflow air, and an analysis of reanalysis data set were performed. We also investigated

Table 4
Same as in Table 3 but for Parameters Estimated From the GEOS-5 FP Reanalysis

Parameters	Anomalous mean (median)	Normal mean (median)	Mann-whitney U-statistic *p* values
Surface Equiv. Pot. Temp.	335 (332) K	340 (342) K	0.2330
Ave. Spec. Hum. Sfc-LCL	8.9 (8.5) g kg^{-1}	10.9 (10.9) g kg^{-1}	0.0609
Ave. Rel. Hum. Sfc-LCL	60 (62) %	65 (65) %	0.1729
LCL height	2521 (2,399) m	2145 (1,908) m	0.2681
Height 0°C	4004 (3,776) m	4655 (4,746) m	**0.0072**
Warm Cloud Depth	1,483 (1,792) m	2510 (2,479) m	**0.0082**
Ave. Spec. Hum. WCD	4.3 (4.6) g kg^{-1}	6.1 (6.1) g kg^{-1}	**0.0192**
Ave. Rel. Hum. WCD	50 (46) %	58 (53) %	0.3463
Precipitable Water	23 (21) mm	29 (27) mm	**0.0253**
Surface CAPE	808 (760) J kg^{-1}	797 (471) J kg^{-1}	0.6389
Most-unstable CAPE	808 (760) J kg^{-1}	1030 (916) J kg^{-1}	0.7655
Wind Shear 0–6 km	34 (36) kt	37 (36) kt	0.8814
Wind Shear 0–3 km	16 (15) kt	18 (18) kt	0.7172

CCN observations from a ground-based instrument, and reanalysis estimates of aerosols that most likely act as CCN, and their possible role on charge structure.

We observed that a set of parameters presented anomalous and normal storm values distinct at a high confidence level and were consistent with the initial hypothesis that contributes to large cloud liquid water content in the mixed-phase layer and anomalous charge structures. Conditions that differentiated anomalous from normal storms are those related to low-level humidity, WCD, and the 0°C isotherm height. Interestingly, no consistent differences between anomalous and normal storms were found for the LCL height, with means slightly higher for anomalous but not at a high confidence level. The dry low-level humidity and small WCD is consistent with the hypothesis that droplet growth would be unfavorable in the warm sector of the cloud due to small droplets residence time in this layer, facilitating more small droplets with similar sizes that can be lifted to the mixed-phase

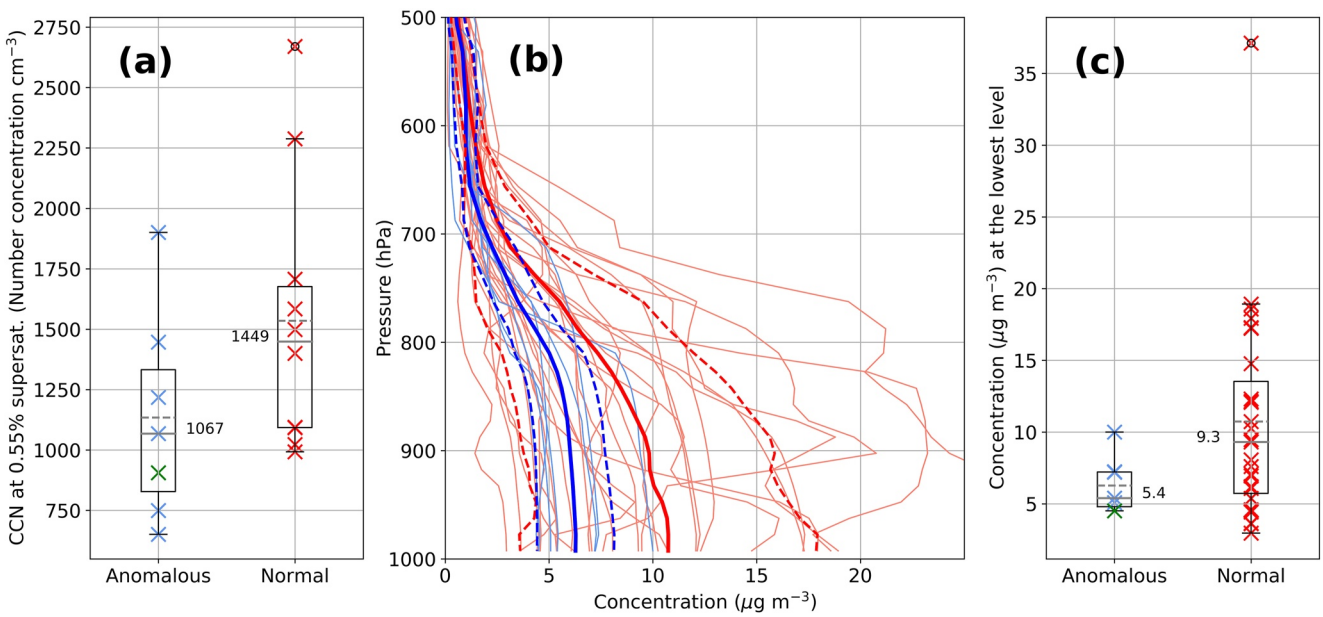

Figure 5. (a) CCN concentration at 0.55% supersaturation in cm^{-3} for a set of seven anomalous and 10 normal events. (b) MERRA-2 aerosol concentration in $\mu g\ m^{-3}$ in relation to pressure levels for each of the anomalous (thin blue line) and normal (thin red line) reanalysis events. Average and standard deviation for each set of events are shown as continuous and dashed thick lines, respectively. (c) MERRA-2 aerosol concentration ($\mu g\ m^{-3}$) for the lowest level.

layer, enhancing cloud liquid water content in this region, and favoring positive charging of graupel in collisions with ice crystals. These results are consistent with other studies of thunderstorm environments in the United States (Carey & Buffalo, 2007; Fuchs et al., 2015, 2018; Williams et al., 2005). Drier WCD for anomalous storms is possibly associated with dry entrainment that suppressed droplet growth, also contributing to more small droplets that can be advected aloft to the mixed-phase layer, inducing anomalous charge structure thunderstorms (Chmielewski et al., 2018).

When analyzing parameters associated with updraft strength from the sounding data set, anomalous storms presented lower CAPE and lower precipitable water than normal storms, and values for anomalous and normal storms for wind shear were not significantly different. As low precipitable water for anomalous storms is thought to be related to less rainwater loading (Carey & Buffalo, 2007; Eddy et al., 2021; Emanuel, 1981; Knupp & Cotton, 1985), that would be associated with stronger updrafts, an opposing effect to the low CAPE observed for these storms, which would induce lower buoyancy and weaker updrafts. To investigate this result, we looked at reanalysis data for a largely different set of storms, and found no distinction for CAPE and wind shear values when comparing normal with anomalous storms, while anomalous storms presented low values for the precipitable water parameter. These results suggest updraft intensity is not a necessary condition for the development of anomalous storms in this region of the world, contrary to other studies that found anomalous storms to be associated with strong updrafts and severe storms (Carey & Buffalo, 2007; Eddy et al., 2021; Fuchs et al., 2015; Ziegler et al., 1991).

In general, results from the GEOS-5 FP reanalysis data agree with the sounding results, but at a lower confidence level. Although the sounding analysis had a smaller data set of events, this behavior was expected as a released sounding should better represent the true environmental air ingested into a convective cloud.

Observations of CCN concentration had not been investigated for a detailed thunderstorm charge structure analysis before, to the best of our knowledge. Our data set size for this analysis was even smaller than the sounding analysis, as this single ground instrument could not be associated with some storms because the availability of the data was not consistent throughout RELAMPAGO-CACTI EOP, and some storms were at a far distance from the instrument. Even so, we observed that the initial hypothesis was rejected, where the CCN mean for anomalous storms was lower than for the normal storms. Verifying this result with a larger and largely different set of storms during RELAMPAGO-CACTI using reanalysis data of aerosol mass concentration led to a similar behavior. This suggests that CCN may not be an important factor for development of anomalous storms in Cordoba, contrary to other study findings (Albrecht et al., 2011; Lyons et al., 1998). Preliminary analysis of the low-level flow indicates that some normal events with larger CCN concentration might have been influenced by southward flow from the polluted Cordoba metro area. In this study we were able to explore both aerosols and humidity conditions independently, which are sometimes interrelated. Hence, we have found that meteorological conditions, including specific humidity, in the low-levels seem to be an important factor that led to anomalous thunderstorms.

The 0°C height influence on WCD leads to a hypothesis that the dominant synoptic conditions may have had an important role for determining the dominant charge structure for thunderstorms during RELAMPAGO-CACTI. For example, the period from 29 November to 5 December 2018 had a predominance of anomalous storms, when half of the anomalous data set storms occurred (Table 1). We analyzed the dominant synoptic conditions in this period and contrasted them with 23–29 January 2019, a period with a predominance of normal charge structure storms (Table 1). From 11/29 to 12/05, a subtropical jet stream was located north of Cordoba (Figure S1a-S1c), which indicates a shallow troposphere south of the high-level jet. The tropopause was at a pressure level of about 250 hPa as observed from soundings during that week, which influenced the lowering of the troposphere thickness. During most of the period, the temperature at 500 hPa was only about −13°C from sounding observations. A passage of a cold front over the area of study occurred on 12/01, and a post-frontal surface high pressure system dominated on the following days (Figure S1h). During late January, a period dominated by normal charge structure thunderstorms, the upper troposphere Bolivian high-pressure system caused by the Amazon forest latent heat release (Lenters & Cook, 1997) was occurring south of its summer climatological position (Figure S2a-S2c). Cordoba was on the equatorial side of the subtropical jet stream, which led to the tropopause being at about 150 hPa as inferred from soundings. That contributed to the tall convection that occurred in this period, with storms top reaching up to 20 km altitude. Southward moisture advection in low-levels from the Amazon in the form of a low-level jet (Vera et al., 2006) led to a region of convergence in Argentina (Figure S2g-S2i), and contributed to high low-level humidity, contrasting with drier low-level humidity for anomalous cases in late

November and early December. These different synoptic conditions could have played an important role in determining the environment of thunderstorms during RELAMPAGO-CACTI, thus impacting the dominant storm processes and charge structures in storms.

The two normal charge structure storms that occurred in late November and early December during the week with predominant anomalous charge structure storms (Table 1) were found to produce the lowest normal values for the following parameters: surface equivalent potential temperature, average specific humidity from the surface to LCL, height of 0°C, WCD, precipitable water, and CAPE parameters (Figure 3). Some of the parameter values for these two events were outliers among the normal data set, and were closer to the anomalous inter-quartile range. For other parameters, values for these events were within the inter-quartile range of both anomalous and normal because these parameters were not distinct to each other. This analysis reinforces the possible role of synoptic conditions to thunderstorm charge structures, as a removal of these two events would cause a more distinct separation of anomalous and normal datasets.

The relation of environment with thunderstorm charge structure is indirect, with in-cloud conditions having a more direct role. These conditions include an investigation of the microphysical and kinematic processes, which are the subject of a future radar-based study. A detailed investigation of the apparently unique characteristics of anomalous thunderstorms in Argentina with enhanced positive charge at temperatures warmer than −10°C is also necessary. An investigation of a larger sample of low-level anomalous charge structures, ideally addressing events in different regions of the world, is encouraged to the community since it would help improve our understanding, terminology, and conceptual model definition for such events.

Data Availability Statement

Radiosonde data is available on the NCAR-Earth Observing Laboratory RELAMPAGO archive on https://data.eol.ucar.edu/master_lists/generated/relampago/. Dual Column CCN Counter data are available on www.arm.gov/research/campaigns/amf2018cacti. RELAMPAGO LMA data are available on https://doi.org/10.5067/RELAMPAGO/LMA/DATA101. The GEOS data used in this study have been provided by the Global Modeling and Assimilation Office (GMAO) at NASA Goddard Space Flight Center through the online data portal in the NASA Center for Climate Simulation. MERRA-2 data is available on https://disc.gsfc.nasa.gov/datasets?project=MERRA-2.

Acknowledgments
We thank the NOAA GOES-R Program and the NASA Lightning Imaging Sensor (LIS) for the RELAMPAGO LMA funding. The first author and coauthors Carey and Bitzer wish to acknowledge support from the National Science Foundation Award AGS 1661785 and NASA MSFC Grant NNM11AA01A.

References

Albrecht, R. I., Morales, C. A., & Silva Dias, M. A. (2011). Electrification of precipitating systems over the Amazon: Physical processes of thunderstorm development. *Journal of Geophysical Research*, *116*(D8), D08209. https://doi.org/10.1029/2010JD014756

Baker, B., Baker, M. B., Jayaratne, E. R., Latham, J., & Saunders, C. P. R. (1987). The influence of diffusional growth rates on the charge transfer accompanying rebounding collisions between ice crystals and soft hailstones. *Quarterly Journal of the Royal Meteorological Society*, *113*(478), 1193–1215. https://doi.org/10.1002/qj.49711347807

Berdeklis, P., & List, R. (2001). The ice crystal–graupel collision charging mechanism of thunderstorm electrification. *Journal of the Atmospheric Sciences*, *58*(18), 2751–2770. https://doi.org/10.1175/1520-0469(2001)058<2751:TICGCC>2.0.CO;2

Bruning, E. C., & MacGorman, D. R. (2013). Theory and observations of controls on lightning flash size spectra. *Journal of the Atmospheric Sciences*, *70*(12), 4012–4029. https://doi.org/10.1175/JAS-D-12-0289.1

Bruning, E. C., Rust, W. D., MacGorman, D. R., Biggerstaff, M. I., & Schuur, T. J. (2010). Formation of charge structures in a supercell. *Monthly Weather Review*, *138*(10), 3740–3761. https://doi.org/10.1175/2010MWR3160.1

Bruning, E. C., Weiss, S. A., & Calhoun, K. M. (2014). Continuous variability in thunderstorm primary electrification and an evaluation of inverted-polarity terminology. *Atmospheric Research*, *135*, 274–284. https://doi.org/10.1016/j.atmosres.2012.10.009

Carey, L. D., & Buffalo, K. M. (2007). Environmental control of cloud-to-ground lightning polarity in severe storms. *Monthly Weather Review*, *135*(4), 1327–1353. https://doi.org/10.1175/MWR3361.1

Carey, L. D., & Rutledge, S. A. (1998). Electrical and multiparameter radar observations of a severe hailstorm. *Journal of Geophysical Research*, *103*(D12), 13979–14000. https://doi.org/10.1029/97JD02626

Carey, L. D., Rutledge, S. A., & Petersen, W. A. (2003). The relationship between severe storm reports and cloud-to-ground lightning polarity in the contiguous United States from 1989 to 1998. *Monthly Weather Review*, *131*(7), 1211–1228. https://doi.org/10.1175/1520-0493(2003)131<1211:TRBSSR>2.0.CO;2

Chmielewski, V. C., Bruning, E. C., & Ancell, B. C. (2018). Variations of thunderstorm charge structures in west Texas on 4 june 2012. *Journal of Geophysical Research: Atmospheres*, *123*(17), 9502–9523. https://doi.org/10.1029/2018JD029006

Curran, E. B., Holle, R. L., & López, R. E. (2000). Lightning casualties and damages in the United States from 1959 to 1994. *Journal of Climate*, *13*(19), 3448–3464. https://doi.org/10.1175/1520-0442(2000)013<3448:LCADIT>2.0.CO;2

Davydenko, S. S., Mareev, E. A., Marshall, T. C., & Stolzenburg, M. (2004). On the calculation of electric fields and currents of mesoscale convective systems. *Journal of Geophysical Research*, *109*(D11), D11103. https://doi.org/10.1029/2003JD003832

DeCaria, A. J., Pickering, K. E., Stenchikov, G. L., & Ott, L. E. (2005). Lightning-generated NOx and its impact on tropospheric ozone production: A three-dimensional modeling study of a stratosphere-troposphere experiment: Radiation, aerosols and ozone (STERAO-A) thunderstorm. *Journal of Geophysical Research*, *110*. D14303. https://doi.org/10.1029/2004JD00555

Dye, J. E., Jones, J. J., Weinheimer, A. J., & Winn, W. P. (1988). Observations within two regions of charge during initial thunderstorm electrification. *Quarterly Journal of the Royal Meteorological Society*, *114*(483), 1271–1290. https://doi.org/10.1002/qj.49711448306

Dye, J. E., Jones, J. J., Winn, W. P., Cerni, T. A., Gardiner, B., Lamb, D., et al. (1986). Early electrification and precipitation development in a small, isolated Montana cumulonimbus. *Journal of Geophysical Research*, *91*(D1), 1231–1247. https://doi.org/10.1029/JD091iD01p01231

Dye, J. E., Winn, W. P., Jones, J. J., & Breed, D. W. (1989). The electrification of New Mexico thunderstorms: 1. Relationship between precipitation development and the onset of electrification. *Journal of Geophysical Research*, *94*(D6), 8643–8656. https://doi.org/10.1029/JD094iD06p08643

Eddy, A. J., MacGorman, D. R., Homeyer, C. R., & Williams, E. (2021). Intraregional comparisons of the near-storm environments of storms dominated by frequent positive versus negative cloud-to-ground flashes. *Earth and Space Science*, *8*(5), e2020EA001141. https://doi.org/10.1029/2020EA001141

Emanuel, K. A. (1981). A similarity theory for unsaturated downdrafts within clouds. *Journal of the Atmospheric Sciences*, *38*(8), 1541–1557. https://doi.org/10.1175/1520-0469(1981)038<1541:ASTFUD>2.0.CO;2

Emersic, C., & Saunders, C. P. R. (2010). Further laboratory investigations into the relative diffusional growth rate theory of thunderstorm electrification. *Atmospheric Research*, *98*(2–4), 327–340. https://doi.org/10.1016/j.atmosres.2010.07.011

Fernandes, W. A., Pinto, I. R., Pinto, O., Jr., Longo, K. M., & Freitas, S. R. (2006). New findings about the influence of smoke from fires on the cloud-to-ground lightning characteristics in the Amazon region. *Geophysical Research Letters*, *33*(20), L20810. https://doi.org/10.1029/2006GL027744

Fuchs, B. R., Rutledge, S. A., Bruning, E. C., Pierce, J. R., Kodros, J. K., Lang, T. J., et al. (2015). Environmental controls on storm intensity and charge structure in multiple regions of the continental United States. *Journal of Geophysical Research: Atmospheres*, *120*(13), 6575–6596. https://doi.org/10.1002/2015JD023271

Fuchs, B. R., Rutledge, S. A., Dolan, B., Carey, L. D., & Schultz, C. (2018). Microphysical and kinematic processes associated with anomalous charge structures in isolated convection. *Journal of Geophysical Research: Atmospheres*, *123*(12), 6505–6528. https://doi.org/10.1029/2017JD027540

Gelaro, R., McCarty, W., Suárez, M. J., Todling, R., Molod, A., Takacs, L., et al. (2017). The modern-era retrospective analysis for research and applications, version 2 (MERRA-2). *Journal of Climate*, *30*(14), 5419–5454. https://doi.org/10.1175/JCLI-D-16-0758.1

Grant, L. D., & van den Heever, S. C. (2015). Cold pool and precipitation responses to aerosol loading: Modulation by dry layers. *Journal of the Atmospheric Sciences*, *72*(4), 1398–1408. https://doi.org/10.1175/JAS-D-14-0260.1

Knupp, K. R., & Cotton, W. R. (1985). Convective cloud downdraft structure: An interpretive survey. *Reviews of Geophysics*, *23*(2), 183–215. https://doi.org/10.1029/RG023i002p00183

Lang, T. J., & Rutledge, S. A. (2011). A framework for the statistical analysis of large radar and lightning datasets: Results from STEPS 2000. *Monthly Weather Review*, *139*(8), 2536–2551. https://doi.org/10.1175/MWR-D-10-05000.1

Lenters, J. D., & Cook, K. H. (1997). On the origin of the Bolivian high and related circulation features of the South American climate. *Journal of the Atmospheric Sciences*, *54*(5), 656–678. https://doi.org/10.1175/1520-0469(1997)054<0656:OTOOTB>2.0.CO;2

Lucchesi, R. (2018). File specification for GEOS FP. *GMAO Office Note No. 4 (Version 1.2)*, 61. Retrieved from: http://gmao.gsfc.nasa.gov/pubs/office_notes

Lyons, W. A., Nelson, T. E., Williams, E. R., Cramer, J. A., & Turner, T. R. (1998). Enhanced positive cloud-to-ground lightning in thunderstorms ingesting smoke from fires. *Science*, *282*(5386), 77–80. https://doi.org/10.1126/science.282.5386.77

MacGorman, D. R., & Burgess, D. W. (1994). Positive cloud-to-ground lightning in tornadic storms and hailstorms. *Monthly Weather Review*, *122*(8), 1671–1697. https://doi.org/10.1175/1520-0493(1994)122<1671:PCTGLI>2.0.CO;2

Marshall, T. C., Rust, W. D., & Stolzenburg, M. (1995). Electrical structure and updraft speeds in thunderstorms over the southern Great Plains. *Journal of Geophysical Research*, *100*(D1), 1001–1015. https://doi.org/10.1029/94JD02607

May, R. M., Arms, S. C., Marsh, P., Bruning, E., Leeman, J. R., Goebbert, K., et al. (2020). MetPy: A Python package for meteorological data. *Version 0.12.1.post2*. Available online at https://github.com/Unidata/MetPy

Medina, B. L., Carey, L. D., Lang, T. J., Bitzer, P. M., Deierling, W., & Zhu, Y. (2021). Characterizing charge structure in central Argentina thunderstorms during RELAMPAGO utilizing a new charge layer polarity identification method. *Earth and Space Science*, *8*, e2021EA001803. https://doi.org/10.1029/2021EA001803

Mulholland, J. P., Peters, J. M., & Morrison, H. (2021). How does LCL height influence deep convective updraft width? *Geophysical Research Letters*, *48*(13), e2021GL093316. https://doi.org/10.1029/2021GL093316

Nesbitt, S. W., Salio, P. V., Avila, E., Bitzer, P., Carey, L., Chandrasekar, V., et al. (2021). A storm safari in subtropical south America: Proyecto RELAMPAGO. *Bulletin of the American Meteorological Society*, *102*(8), 1–64. https://doi.org/10.1175/BAMS-D-20-0029.1

Pereyra, R. G., Avila, E. E., Castellano, N. E., & Saunders, C. P. (2000). A laboratory study of graupel charging. *Journal of Geophysical Research*, *105*(D16), 20803–20812. https://doi.org/10.1029/2000JD900244

Price, C., Penner, J., & Prather, M. (1997). NOx from lightning: 1. Global distribution based on lightning physics. *Journal of Geophysical Research*, *102*(D5), 5929–5941. https://doi.org/10.1029/96JD03504

Qie, X., Zhang, T., Chen, C., Zhang, G., Zhang, T., & Wei, W. (2005). The lower positive charge center and its effect on lightning discharges on the Tibetan Plateau. *Geophysical Research Letters*, *32*(5), L05814. https://doi.org/10.1029/2004GL022162

Rust, W. D., & MacGorman, D. R. (2002). Possibly inverted-polarity electrical structures in thunderstorms during STEPS. *Geophysical Research Letters*, *29*(12), 12–1. https://doi.org/10.1029/2001GL014303

Rust, W. D., MacGorman, D. R., Bruning, E. C., Weiss, S. A., Krehbiel, P. R., Thomas, R. J., et al. (2005). Inverted-polarity electrical structures in thunderstorms in the severe thunderstorm electrification and precipitation study (STEPS). *Atmospheric Research*, *76*(1–4), 247–271. https://doi.org/10.1016/j.atmosres.2004.11.029

Saunders, C. P. R., Keith, K. W., & Mitzeva, R. P. (1991). The effect of liquid water on thunderstorm charging. *Journal of Geophysical Research*, *96*(D6), 11007–11017. https://doi.org/10.1029/91JD00970

Saunders, C. P. R., & Peck, S. L. (1998). Laboratory studies of the influence of the rime accretion rate on charge transfer during crystal/graupel collisions. *Journal of Geophysical Research*, *103*(D12), 13949–13956. https://doi.org/10.1029/97JD02644

Saunders, C. P. R., Peck, S. L., Varela, G. A., Avila, E. E., & Castellano, N. E. (2001). A laboratory study of the influence of water vapour and mixing on the charge transfer process during collisions between ice crystals and graupel. *Atmospheric Research*, *58*(3), 187–203. https://doi.org/10.1016/S0169-8095(01)00090-4

Schumacher, R. S., Hence, D. A., Nesbitt, S. W., Trapp, R. J., Kosiba, K. A., Wurman, J., et al. (2021). Convective-storm environments in subtropical South America from high-frequency soundings during RELAMPAGO-CACTI. *Monthly Weather Review*, *149*(5), 1439–1458. https://doi.org/10.1175/MWR-D-20-0293.1

Smith, S. B., LaDue, J. G., & MacGorman, D. R. (2000). The relationship between cloud-to-ground lightning polarity and surface equivalent potential temperature during three tornadic outbreaks. *Monthly Weather Review*, *128*(9), 3320–3328. https://doi.org/10.1175/1520-0493(2000)128<3320:TRBCTG>2.0.CO;2

Stephens, M. A. (1974). EDF statistics for goodness of fit and some comparisons. *Journal of the American Statistical Association*, *69*(347), 730–737. https://doi.org/10.1080/01621459.1974.10480196

Stolzenburg, M., & Marshall, T. C. (2008). Charge structure and dynamics in thunderstorms. *Space Science Reviews*, *137*(1), 355–372. https://doi.org/10.1007/s11214-008-9338-z

Stolzenburg, M., Rust, W. D., & Marshall, T. C. (1998). Electrical structure in thunderstorm convective regions: 2. Isolated storms. *Journal of Geophysical Research*, *103*(D12), 14079–14096. https://doi.org/10.1029/97JD03547

Stolzenburg, M., Rust, W. D., Smull, B. F., & Marshall, T. C. (1998). Electrical structure in thunderstorm convective regions: 1. Mesoscale convective systems. *Journal of Geophysical Research*, *103*(D12), 14059–14078. https://doi.org/10.1029/97JD03546

Stough, S. M., Carey, L. D., Schultz, C. J., & Cecil, D. J. (2021). Examining conditions supporting the development of anomalous charge structures in supercell thunderstorms in the Southeastern United States. *Journal of Geophysical Research: Atmospheres*(16). In press. https://doi.org/10.1029/2021JD034582

Takahashi, T. (1978). Riming electrification as a charge generation mechanism in thunderstorms. *Journal of the Atmospheric Sciences*, *35*(8), 1536–1548. https://doi.org/10.1175/1520-0469(1978)035<1536:REAACG>2.0.CO;2

UCAR/NCAR–Earth Observing Laboratory. (2020). *Multi-network composite 5 mb vertical resolution sounding composite*, version 1.3. Accessed 27 May 2020. https://doi.org/10.26023/EXZJ-XBEV-KV05

Uin, J., Salwen, C., & Senum, G. (2018). Cloud condensation nuclei particle counter (AOSCCN2COLAAVG). *Atmospheric Radiation Measurement (ARM) user facility* Accessed 3 February 2021.

Varble, A. C., Nesbitt, S. W., Salio, P., Hardin, J. C., Bharadwaj, N., Borque, P., et al. (2021). Utilizing a storm-generating hotspot to study convective cloud transitions: The CACTI experiment. *Bulletin of the American Meteorological Society*, *102*(8), 1–67. https://doi.org/10.1175/BAMS-D-20-0030.1

Vera, C., Baez, J., Douglas, M., Emmanuel, C. B., Marengo, J., Meitin, J., et al. (2006). The South American low-level jet experiment. *Bulletin of the American Meteorological Society*, *87*(1), 63–78. https://doi.org/10.1175/BAMS-87-1-63

Wilks, D. S. (2011). *Statistical Methods in the Atmospheric Sciences* (Vol. 100). Academic press.

Williams, E., Mushtak, V., Rosenfeld, D., Goodman, S., & Boccippio, D. (2005). Thermodynamic conditions favorable to superlative thunderstorm updraft, mixed phase microphysics and lightning flash rate. *Atmospheric Research*, *76*(1–4), 288–306. https://doi.org/10.1016/j.atmosres.2004.11.009

Williams, E. R. (1985). Large-scale charge separation in thunderclouds. *Journal of Geophysical Research*, *90*(D4), 6013–6025. https://doi.org/10.1029/JD090iD04p06013

Williams, E. R., Zhang, R., & Rydock, J. (1991). Mixed-phase microphysics and cloud electrification. *Journal of the Atmospheric Sciences*, *48*(19), 2195–2203. https://doi.org/10.1175/1520-0469(1991)048<2195:MPMACE>2.0.CO;2

Ziegler, C. L., MacGorman, D. R., Dye, J. E., & Ray, P. S. (1991). A model evaluation of noninductive graupel-ice charging in the early electrification of a mountain thunderstorm. *Journal of Geophysical Research*, *96*(D7), 12833–12855. https://doi.org/10.1029/91JD01246

Zipser, E. J., Cecil, D. J., Liu, C., Nesbitt, S. W., & Yorty, D. P. (2006). Where are the most intense thunderstorms on Earth? *Bulletin of the American Meteorological Society*, *87*(8), 1057–1072. https://doi.org/10.1175/BAMS-87-8-1057